Graphene Oxide as Support for Layered Double Hydroxides:Enhancing the CO2 Adsorption Capacity

DATASET *in* CHEMISTRY OF MATERIALS · JUNE 2013

Impact Factor: 8.35

10 AUTHORS, INCLUDING:

Ainara García
Bio Nano Consulting
29 PUBLICATIONS **206** CITATIONS
SEE PROFILE

Abdullah M. Asiri
King Abdulaziz University
1,166 PUBLICATIONS **6,889** CITATIONS
SEE PROFILE

Shaeel Al-thabaiti
King Abdulaziz University
221 PUBLICATIONS **990** CITATIONS
SEE PROFILE

Abdulrahman Al-youbi
King Abdulaziz University
223 PUBLICATIONS **2,622** CITATIONS
SEE PROFILE

CHEMISTRY OF MATERIALS

Article

pubs.acs.org/cm

Graphene Oxide as Support for Layered Double Hydroxides: Enhancing the CO_2 Adsorption Capacity

Ainara Garcia-Gallastegui,*[,†,‡] Diana Iruretagoyena,[‖] Veronica Gouvea,[†] Mohamed Mokhtar,[§] Abdullah M. Asiri,[§] Sulaiman N. Basahel,[§] Shaeel A. Al-Thabaiti,[§] Abdulrahman O. Alyoubi,[§] David Chadwick,[‖] and Milo S. P. Shaffer*[,†]

[†]Department of Chemistry and [‖]Department of Chemical Engineering, Imperial College London, South Kensington Campus, London SW7 2AZ, U.K.

[‡]Bio Nano Consulting, 338 Euston Road, London NW1 3BT, U.K.

[§]Department of Chemistry, Faculty of Science, King Abdulaziz University, Jeddah 21589, Saudi Arabia

Supporting Information

ABSTRACT: Layered double hydroxides (LDHs) show great potential as CO_2 adsorbent materials, but require improvements in stability and CO_2 adsorption capacity for commercial applications. In the current study, graphene oxide provides a light-weight, charge-complementary, two-dimensional (2D) material that interacts effectively with the 2D LDHs, in turn enhancing the CO_2 uptake capacity and multicycle stability of the assembly. As a result, the absolute capacity of the LDH was increased by 62% using only 7 wt % graphene oxide (GO) as a support. The experimental procedure for the synthesis of the materials is based on a direct precipitation of the LDH nanoparticles onto GO followed by a structural and physical characterization by electron microscopy, X-ray diffraction, thermogravimetric analysis, and Brunauer–Emmett–Teller (BET) surface area measurements. Detailed titration confirmed the compatibility of the surface chemistry. After thermal decomposition, mixed metal oxides (MMOs) are obtained with the basic sites required for the CO_2 adsorption. A range of samples with different proportions of GO/MMO were prepared, fully characterized, and correlated with the CO_2 sorption capacity, established via TGA.

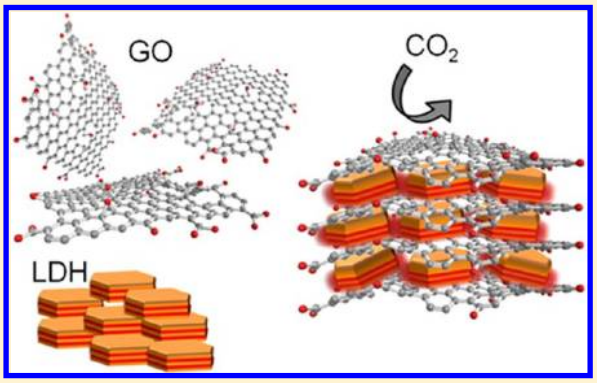

KEYWORDS: *graphene oxide (GO), graphene, layered double hydroxide(s) (LDHs), hydrotalcite(s), CO_2 sorption, CO_2 capture and storage (CCS)*

1. INTRODUCTION

Graphene and its potential applications are receiving intense attention, driven by its unique chemical and physical properties. Nominally, ideal graphene has an extremely large surface area (up to 2630 $m^2\ g^{-1}$), high strength and stiffness, impressive electronic properties (charge-carrier mobility of 250000 $cm^2\ V^{-1}\ s^{-1}$ at room temperature), and high thermal conductivity (5000 $W\ m^{-1}\ K^{-1}$).[1] As a result, graphene has been widely explored in a variety of applications including field-effect transistors, ultrasensitive sensors, fuel cells, electromechanical resonators, and supercapacitors, to name a few.[2] On the other hand, real graphenes that are processed in bulk, produced for example by chemical exfoliation methods, tend to have less impressive performance than expected because of damage, restacking, or other processing limitations. Graphene Oxide (GO) is commonly used as a water-soluble precursor to graphene,[3] despite the intrinsically degraded nature of the final product. It is particularly interesting, therefore, to identify contexts in which the surface chemistry (and flat geometry) of GO is actively desirable. One attractive possibility is as a support for the growth of other layered two-dimensional (2D) inorganic materials.

Layered double hydroxides (LDHs), also known as hydrotalcite-like compounds, are inorganic materials with unique basic properties relevant to diverse applications. LDHs belong to a large class of synthetic 2D nanostructured basic, anionic clays. Their structure is composed of positively charged brucite-like $Mg(OH)_2$ layers in which a fraction of divalent cations, octahedrally coordinated by hydroxyls, are partially substituted by trivalent cations. The excess of positive charge is balanced by intercalated anions, and loosely bound water molecules may occupy the remaining free space in the interlayer regions. The charge-neutral LDH structure can be represented by the general formula

$$(M^{2+}_{1-x}M^{3+}_{x}(OH)_2)^{x+}(A^{m-}_{x/m}\cdot nH_2O)^{x-}$$

Received: June 12, 2012
Revised: September 10, 2012
Published: October 29, 2012

   dx.doi.org/10.1021/cm3018264 | *Chem. Mater.* 2012, 24, 4531–4539

where M^{2+}, M^{3+}, and A^{m-} commonly represent Mg^{2+}, Al^{3+}, and CO_3^{2-}, respectively, and x is usually between 0.17 and 0.33.

LDHs have shown promise as CO_2 adsorbent materials, providing an attractive possible solid state alternative to current carbon capture and storage (CCS) technologies. LDHs require less energy for regeneration and show better multicycle stability than other CO_2 solid adsorbents (e.g., calcium oxides).[4] In addition, they exhibit fast adsorption−desorption kinetics, particularly in the presence of water, making them very attractive not only for precombustion capture applications but also for sorption-enhanced hydrogen production.[5−8] Despite these positive adsorption properties, LDHs exhibit relatively low CO_2 adsorption capacities. Recently, we reported that the CO_2 adsorption performance of LDHs is considerably enhanced when supported on oxidized multiwalled carbon nanotubes (MWNTs).[9] However, the 2D geometry of GO is more obviously compatible with LDHs, while the surface chemistry is expected to be similarly favorable. In principle, a single, atomically thin layer of GO may stabilize LDH platelets on each side, suggesting a very high mass efficiency as a support; the large size of GO sheets compared to LDH platelets implies that it may be possible to form an open network with large pores allowing access to the active LDH. For these reasons, we have investigated GO as an ideal 2D support for LDHs.

Related hybrid materials have been synthesized for other applications.[10] GO and LDH have been assembled with poly(vinyl alcohol) (PVA) for potential applications in electrodes and multifunctional nanocomposites.[11] The hybrid was used to remove arsenate from solutions when combined with magnetite particles,[12] and has been considered also for electrocatalysis[13] among other applications.[14−19] In addition, the introduction of LDH particles can enhance the performance of graphene-based electrodes in supercapacitors.[20−24] In general, unavoidable aggregation or restacking of graphene nanosheets reduces capacitance; separating and supplementing the graphene sheets by loading (electrochemically active) LDH materials is attractive.

Herein, we report a facile and low temperature method for the preparation of LDH/GO hybrids by in situ coprecipitation of LDH onto GO, in aqueous dispersion. The effect of the GO content in the LDH/GO hybrid has been studied and fully characterized. Thermal treatment of the LDH/GO hybrids results in the formation of mixed metal oxides (MMOs) with the basic sites required for the CO_2 adsorption. For the first time, to the authors' knowledge, the influence of the GO on the CO_2 sorption capacity of such hybrids and their stability under adsorption−desorption cycling is reported. Both materials form planar sheets but with complementary surface charge under relevant conditions (GO negative, LDH positive). The hypothesis studied was that the geometric and charge compatibility between GO and LDH improves the active sorbent morphology, dispersion, and stability, and in turn enhances the CO_2 uptake capacity.

2. EXPERIMENTAL DETAILS

2.1. Materials. Graphene oxide (GO) was purchased from Nanoinnova Technologies, S.L. with a lateral average size and thickness in the range of 1 to 4 μm and 0.7 to 1.2 nm, respectively. $Mg(NO_3)_2{\cdot}6H_2O$ (99%) and $Al(NO_3)_3{\cdot}9H_2O$ (98%) were purchased from Sigma-Aldrich; NaOH was purchased from AnalaR and Na_2CO_3 was purchased from Riedel-de Haen. Polycarbonate membranes were obtained from Millipore (HTTP Isopore membrane).

2.2. Synthesis of Mg−Al LDHs. Unsupported LDHs were prepared via coprecipitation. An Mg/Al ratio of 2 was selected as it has been reported to be optimal for CO_2 sorption.[25] An aqueous solution (50 mL) of 0.1 mol $Mg(NO_3)_2{\cdot}6H_2O$ and 0.05 mol $Al(NO_3)_3{\cdot}9H_2O$ was added to an aqueous solution (75 mL) containing 0.35 mol of NaOH and 0.09 mol of Na_2CO_3. The resulting white suspension was heated at 333 K for 12 h under stirring (300 rpm). The measured pH of the solution was 10. The precipitate was filtered using 0.4 μm polycarbonate membranes and washed with 500 mL of water at 333 K. The sample was dried for 12 h at 393 K. Thermogravimetric analysis (TGA), Energy Dispersive X-Ray Spectroscopy (EDS), and Inductively Coupled Plasma Atomic Emission Spectroscopy (ICP-AES) data were used to determine the molecular formula of the dehydrated sample, which can be expressed as follows: $Mg_{0.67}$ $Al_{0.33}$ $(OH)_2(CO_3)_{0.15}{\cdot}nH_2O$; where the water content estimated from the TGA corresponds to n = 0.5 mol. No measurable sodium content was found by EDS.

2.3. Preparation of Nanostructured LDH/GO Hybrids. A colloidal dispersion of negatively charged GO nanosheets was obtained by dispersing 100 mg of GO in an aqueous solution containing 4.8 M NaOH and 1.2 M Na_2CO_3. Subsequently, a salt solution of 2 M $Mg(NO_3)_2{\cdot}6H_2O$ and 1 M $Al(NO_3)_3{\cdot}9H_2O$ was added. The resulting black suspension was aged at 333 K for 12 h under stirring (300 rpm). The sample was filtered, washed and dried, as explained earlier (section 2.2), for the preparation of unsupported LDHs. Four different LDH/GO hybrids were prepared containing varying GO weight percentages [LDH/GO mass ratios] of 91 wt % [0.1/1], 50 wt % [1/1], 9 wt % [10/1], and 5 wt % [20/1]. These adsorbents were obtained by varying the volume of the basic and nitrate solutions while maintaining a constant mass of GO. The thickness of one LDH platelet is around 10 nm estimated by X-ray diffraction (XRD) broadening and corroborated by transmission electron microscopy (TEM), as shown in the results. The thickness of one single GO sheet as specified by the supplier is about 0.7 to 1.2 nm. Considering that the densities of both materials are of the same order of magnitude (2.25 g cm^{-3} for GO and 2.06 g cm^{-3} for LDH), the microstructures of the samples were expected to follow the trends illustrated (Scheme 1).

Scheme 1. Schematic Representation of the LDH and GO at Different Mass Ratios Highlighting the Degree of Surface Coverage Expected[a]

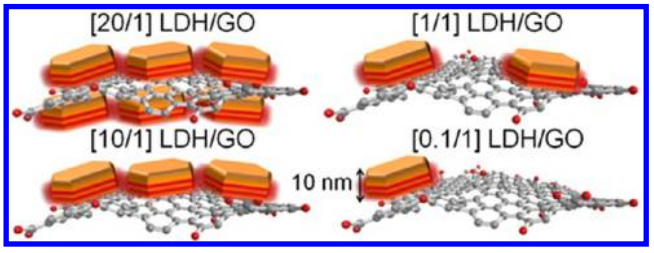

[a]Note that the GO and LDH structures are not drawn to scale.

The LDH/GO mass ratio of [20/1] was selected to provide (approximately) a double-sided coating of LDH on each GO flake; [10/1] is sufficient for a single-sided coating, becoming progressively more dilute at LDH/GO [1/1] (5% coverage) and [0.1/1] (0.5% coverage).

2.4. Calcination of Nanostructured LDH/GO Hybrids. All the materials were calcined prior to CO_2 adsorption measurements at 673 K during 4 h flowing 100 mL min^{-1} N_2, in a quartz tube (ID = 5 cm) heated in a horizontal Carbolite furnace. Calcination at 673 K has been reported to produce LDHs derivatives with an optimum balance between surface area and basic sites needed for CO_2 adsorption.[26] Other reasons for this choice of temperature are discussed below.

2.5. GO Titration. The carboxylic acid group concentration in the as-synthesized GO samples was estimated by adapting the modified Boehm titration procedure established for nanotubes.[27,28] As exemplified in Scheme 2, 50 mg of GO was stirred in 50 mL of

dx.doi.org/10.1021/cm3018264 | Chem. Mater. 2012, 24, 4531−4539

Scheme 2. Carboxylic Acid Group Titration of GO, Using Weak Base

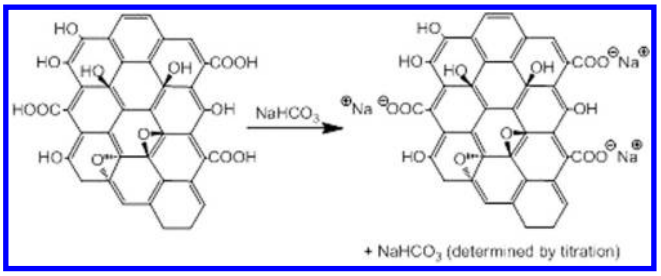

0.05 M $NaHCO_3$ aqueous solution under nitrogen for 2 days. After filtration of the mixture and washing with deionized water, the combined filtrate and washings were added to 50 mL of 0.05 M HCl. The excess of HCl in the solution was titrated with 0.05 M NaOH to neutral, as monitored by a pH meter.

2.6. Measurements and Characterization. Thermogravimetric analysis (TGA) was performed using a Netzsch STA449C. Five mg samples were first dried at 393 K under N_2 for 20 min and then heated from 393 to 1273 at 10 K min^{-1} in 20 mL min^{-1} of air. X-ray diffraction (XRD) tests were conducted using a PAnalytical X'Pert Pro Multi Purpose Diffractometer (Cu K_α radiation) in reflection mode, at room temperature, with 2θ varying between 5° and 80°. High resolution transmission electron microscopy (HRTEM) images were obtained on a JEOL 2010, operating at 200 kV. Samples were prepared by dispersing the sample in isopropanol using 0.01 mg of LDH/GO per mL of solvent, and allowing a drop to dry onto a holey carbon copper grid (300 mesh, Agar Scientific). Scanning Electron Microscopy (SEM) images were collected using Gemini 1525 FEGSEM, fitted with an Oxford Instruments INCA energy dispersive X-ray spectrometer (EDS). Scanning electron microscopy (SEM) images represent bulk dried powder whereas, for HRTEM, LDH/GO material was first dispersed in isopropanol. Nitrogen adsorption and desorption isotherms were measured at 77 K using a Micromeritics Tristar 3000 apparatus on 100 mg of LDH/GO samples, both as-synthesized and calcined, dried at 383 K and held overnight under N_2 prior to adsorption measurements. Specific surface areas were calculated according to the Brunauer–Emmett–Teller (BET) equation. The pore-size distribution of LDH/GO samples was calculated from desorption branch using the Barrett–Joyner–Halenda method.

2.7. CO_2 Adsorption Measurements. A thermogravimetric analyzer (TA Instruments, TAQ500) was used to determine the adsorption capacity of precalcined samples. An amount (~5 mg) of adsorbent was activated in situ to remove CO_2 captured from the atmosphere during storage and transportation. In a typical measurement, the sample was heated from room temperature to 673 at 10 K min^{-1} in a N_2 flow (60 mL min^{-1}) and held for 1 h. The temperature was then decreased to the required adsorption temperature (573 K), and the feed was switched to a 20% CO_2/N_2 premixed gas (BOC), and held for 2 h. The adsorption capacity of the materials was determined from the change in mass during the adsorption step. Effects due to changes in gas viscosity and gas density were taken into account by measuring the response of silicon carbide and then subtracting it from that of the adsorbent. Under the operating conditions used, this blank response was very small. The regeneration and stability of the adsorbents were assessed by multicycle tests, in which the adsorption step was carried out at 573 K for 1 h in a flow of the premixed CO_2 gas; the desorption step was performed at 673 K during 30 min of flowing nitrogen. The flow rate was kept constant at 60 mL min^{-1} during the experiment.

3. RESULTS AND DISCUSSION

During the in situ Mg–Al LDH coprecipitation, the GO sheets are highly negatively charged, as a result of ionization (in the aqueous base) of surface oxide groups, particularly carboxylic acids. This negative charge is complementary to the intrinsic positive charge of the LDH layers and is likely to contribute to the stabilization of the growing hydroxide material. Chemical interactions between the alkaline earth metal ions and GO have been observed elsewhere,[29] and may be particularly relevant to heterogeneous nucleation effects. In any case, the ability of the GO to stabilize the adjacent LDH layer must depend on the relative charge density of the two layered materials. To understand these interactions, quantification of the surface acid group concentration on GO was performed by titration. Using the sodium bicarbonate analysis of carboxylic acid groups in the GO, depicted in the Scheme 2, we estimated a concentration of 1.23 mmol g^{-1}. The ideal surface area of completely exfoliated GO is estimated[30] to be 2630 m^2 g^{-1}. However, the surface area, calculated from the nitrogen adsorption and desorption isotherms of the dried GO sample, is 55.8 m^2 g^{-1}, due to restacking during drying. Therefore, depending on the degree of GO exfoliation, the surface charge density can be within the range of 0.47 (μmol e^-) m^{-2} to 22 (μmol e^-) m^{-2} (or 0.04 C m^{-2} to 2 C m^{-2}) calculated for GO surface areas of 2630 m^2 g^{-1} and 55.8 m^2 g^{-1}, respectively. In the case of the LDH, the extra positive charge due to the Al^{3+} substitution is equivalent to 0.33e per mol of LDH, within the area of the octahedral unit = $\sqrt{3}(a^2/2)$ corresponding[31] to 8.067 Å^2. Consequently, the excess LDH surface charge density is around 6.7 (μmol e^+) m^{-2} (0.6 C m^{-2}). In the typical LDH structure, this positive charge is balanced by anions (mostly carbonates); however, it is clear that the negative surface charge density on the GO is of the same order of magnitude. Thus, the expectation that the LDH should nucleate on, and remain associated with the GO surface, is reasonable.

The XRD patterns of all the LDH-containing samples (Figure 1) display the characteristic reflections corresponding to 2D hydrotalcite-like materials (JCPDS No. 14–191) and can be indexed accordingly.[32] The GO reflection at 11.3° is indexed

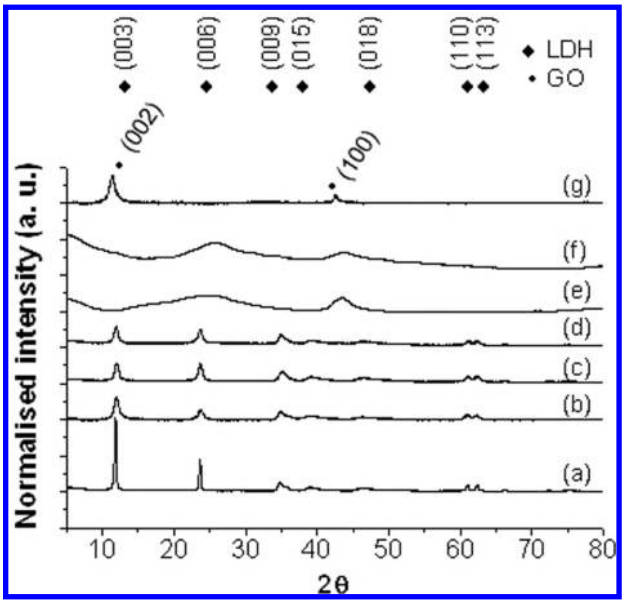

Figure 1. XRD diffraction patterns of (a) unsupported LDH, (b) [20/1] LDH/GO (5 wt % GO), (c) [10/1] LDH/GO (9 wt % GO), (d) [1/1] LDH/GO (50 wt % GO), (e) [0.1/1] LDH/GO (91 wt % GO), (f) Hydrothermally treated GO, and (g) as synthesized GO. (a), (b), (c), and (d) are normalized to the (110) peak of the LDH; (e), (f), and (g) are magnified by a factor of 5.

dx.doi.org/10.1021/cm3018264 | Chem. Mater. 2012, 24, 4531–4539

Table 1. Nominal and Actual Loading and Textural Data of the As-Synthesised LDH/GO Hybrids and, BET Surface Area and CO_2 Sorption Capacity of the Calcined LDH/GO Hybrids

LDH/GO [wt/wt]		wt% GO				
nom	actual	nom	actual	BET surface area (m^2/g)	crystallite size[a] (nm)	($molCO_2$/kg adsorbent)
LDH	LDH	0	0	98.3 ± 0.08	29.9	0.28 ± 0.01
20/1	13.3/1	5	7	149.9 ± 0.35	10.3	0.45 ± 0.02
10/1	7.3/1	9	12	139.3 ± 0.54	11.6	0.38 ± 0.08
1/1	2/1	50	33	61.5 ± 0.13	10.8	0.30 ± 0.07
0.1/1	0.2/1	91	83	5.6 ± 0.11		0.10 ± 0.03
H-GO	GO	100	100	0.1 ± 0.01		

[a]Standard deviation of the mean 0.5.

to the (002) plane. The basal reflection of the LDH corresponding to (003) appears at around the same 2θ angle, 11.8°, overlapping with the GO characteristic peak. The breadth of the 11° peak increases in the hybrids, eventually disappearing, for the 91 wt % GO sample. The increased breadth of the peaks on introducing GO is not simply a linear diffraction contribution from the GO phase; broadening occurs even for small GO additions, and to all interlayer-related LDH peaks. The effect can be attributed to a decrease in the apparent size, or coherence length, in the *c*-direction (layer-stacking direction) from 30 nm in the unsupported LDH to around 10 nm in all the supported LDH/GO samples (estimated by the Scherrer equation) as shown in Table 1. The electrostatic interactions between GO and LDH during the synthesis may affect the nucleation and in turn the crystallite size of the LDH. Similar results were observed when supporting the LDH onto multiwalled carbon nanotubes (MWNTs).[9]

The GO is associated with oxidative debris generated in the original oxidation process. This oxidative debris may act as a surfactant to stabilize aqueous GO suspensions, by coating less oxidized graphene layers with more polar material; however, the debris is expected to become independently solubilized under basic conditions,[33] such as those of the hydrothermal treatment and LDH coprecipitation. In fact, a brown liquid was observed passing through the 0.4 μm filter membrane when washing the LDH after the in situ coprecipitation synthesis in the presence of GO. This brown washing liquid is consistent with previous observation of GO debris, which is thought to consist of fragments of polyaromatic hydrocarbons (also known as carboxylated carbonaceous fragments), functionalized with acidic oxides; these acidic groups become conjugate bases at high pH, increasing their water solubility, and allowing their filtration.[33] To confirm this interpretation, a hydrothermal treatment was performed in the absence of LDH metal precursors, stirring the GO in water at pH 10 for 12 h; a brown solution was again separated from the GO. This hydrothermally treated GO (labeled H-GO below) acts as a useful control sample.

The XRD data suggest that after the removal of the GO debris, the remaining graphitic material restacks. The original, sharp GO peak at 11.3° (Figure 1g), corresponding to an interlayer distance of 0.78 nm, completely disappears after hydrothermal treatment and washing (Figure 1f). Instead, a broad peak appears at 27.1°, corresponding to a graphitic interlayer spacing of about 0.33 nm. This broad peak may be attributed to disordered restacking of exfoliated, partially oxidized graphene sheets remaining after the elimination of the more oxidized debris, by filtration under basic conditions.[33] Hydrothermal reduction of the GO is unlikely since higher temperatures than the 333 K employed during the synthesis of the LDH are required.[34,3514] On introducing a small amount of LDH (9 wt %), the degree of restacking is reduced (broader restacked graphitic (002) peak in Figure 1e than 1f). Restacking is likely further suppressed at higher LDH content due to mutual interactions between the phases; the lack of restacked GO (002) in the higher LDH loading samples (particularly Figure 1c) is consistent with this suggestion but not conclusive because of the low intensity of the GO diffraction.

The TGA (Figure 2) of the original GO has a weight loss at around 500 K because of the decomposition of functional

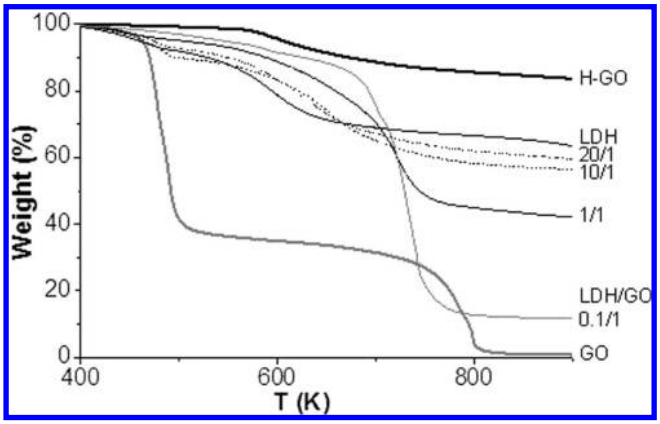

Figure 2. Thermograms of unsupported LDH and LDH/GO hybrid samples. The nominal loading is indicated in the figure, and the deduced actual loading data are in Table 1. Repeated sample traces indicated negligible error.

groups and the oxidation debris; the weight loss at around 750 K has been attributed to the combustion of the (damaged) graphitic regions.[33] The hydrothermally treated GO (H-GO) has a total weight loss of 15%, which is likely to be due to the loss of the functional groups. Assuming that these functional groups are carboxylic acids, a simple correlation with the molecular weight provides an estimate of the concentration to be 3 mmol g^{-1}; this value is of the same order of magnitude as that estimated by titration, although slightly higher as expected, since the thermal degradation involves a range of oxygen-containing groups not just carboxylic acids. The lack of further weight loss is surprising but may be attributed to gas diffusion limitations after restacking; it is worth nothing that the surface area of GO drops from 55.8 m^2 g^{-1} to nearly zero for H-GO (Figure 5). The LDH TGA presents two stages of weight loss. The first weight loss, at approximately 483 K, is attributed to the removal of loosely bound water molecules from the LDH interlayer. The second weight loss, in the temperature range 483−733 K, is due to the removal of OH^- groups and

dx.doi.org/10.1021/cm3018264 | *Chem. Mater.* 2012, 24, 4531−4539

decarbonation of carbonate anions present in the interlayer space. In the hybrid samples this second feature overlaps with the decomposition of the GO. Nevertheless, the actual LDH weight percentage in the sample can be estimated from the residue of each sample. The TGA residue of the unsupported LDH material is composed of ~60 wt % mixed solid oxides, while the residue of GO can be considered negligible. The presence of the LDH will disperse the GO over a large surface area, allowing full combustion, unlike the restacked H-GO sample; thus the GO thermogram is more representative of the combustion of the hybrids. The nominal and actual weight loadings differ slightly as indicated in Table 1. The higher LDH content samples have relatively less LDH than expected probably because the concentration of GO is insufficient to trap all the LDH efficiently on the filter (the flake size of the GO is much greater than the LDH). In contrast, the lower LDH loading samples have relatively more LDH than expected; in this case, the LDH is well trapped by the GO, and the loss of GO oxidation debris during filtering dominates.

HRTEM images showed GO nanosheets with flake-like morphologies spanning the holey-carbon-film. In general, the GO nanosheets form multilayer agglomerates. The HRTEM images shown in Figure 3 reveal typical small, crystalline, hexagonal platelets of LDH attached to the GO nanosheets; interestingly, most LDH platelets were observed to be oriented face-on (i.e., with *ab* faces parallel) to the graphene substrate. In accordance with the XRD results, the thickness of the LDH platelets was found to be 10 nm (Figure 3a). The LDH particles have an average lateral size of 30 nm and are supported on larger GO flakes (1 to 4 μm estimated by the supplier using Atomic Force Microscopy). In situ EDS analysis (see Supporting Information), confirmed the presence of Mg and Al, with an average Mg/Al ratio of 1.9 ± 0.05, close to the intended ratio of 2, and corroborated by ICP-AES for selected samples (not shown). It seems that the interaction between the positively charged LDH sheets and the negatively charged GO successfully led to the deposition of LDHs on the support during the synthesis. SEM analysis (Figure 4) of the dried LDH/GO powder shows LDH particles supported onto micrometric GO layers. As expected, an increase in the number of particles was observed, with increasing weight percentage of LDH. No morphological differences were apparent at the microscale between the as-synthesized and the calcined samples.

Surface area measurements show type IV isotherms according to the IUPAC classification (see Supporting Information), representing a mesoporous adsorbent with strong adsorbent–adsorbate interaction, as observed for the LDH/MWNT hybrids synthesized previously.[9] The surface area of the original GO, measured by BET adsorption, was found to be 55.8 $m^2\ g^{-1}$. The elimination of the oxidation debris and subsequent restacking during the hydrothermal treatment process reduces the BET surface area to 0.013 $m^2\ g^{-1}$. As the surface area of the hybrids increased consistently with increasing LDH content, it can be deduced that the GO restacking is reduced by the alternative LDH/GO stacking interactions (Figure 5). The oxidation debris, assumed to stabilize the GO layers, may be substituted by the LDH particles. As noted above, in the [0.1/1] LDH/GO sample, there is insufficient material to prevent substantial restacking. Upon calcination, the surface area of the unsupported LDH increases from the original 60.23 $m^2\ g^{-1}$ to 98.3 $m^2\ g^{-1}$; similar trends are observed in the LDH/GO hybrids, with a stronger relative effect for higher LDH content. The higher surface areas of the [20/1] and [10/1] hybrids can be related to the reduced thickness of the LDH (see crystallite size in Table 1).

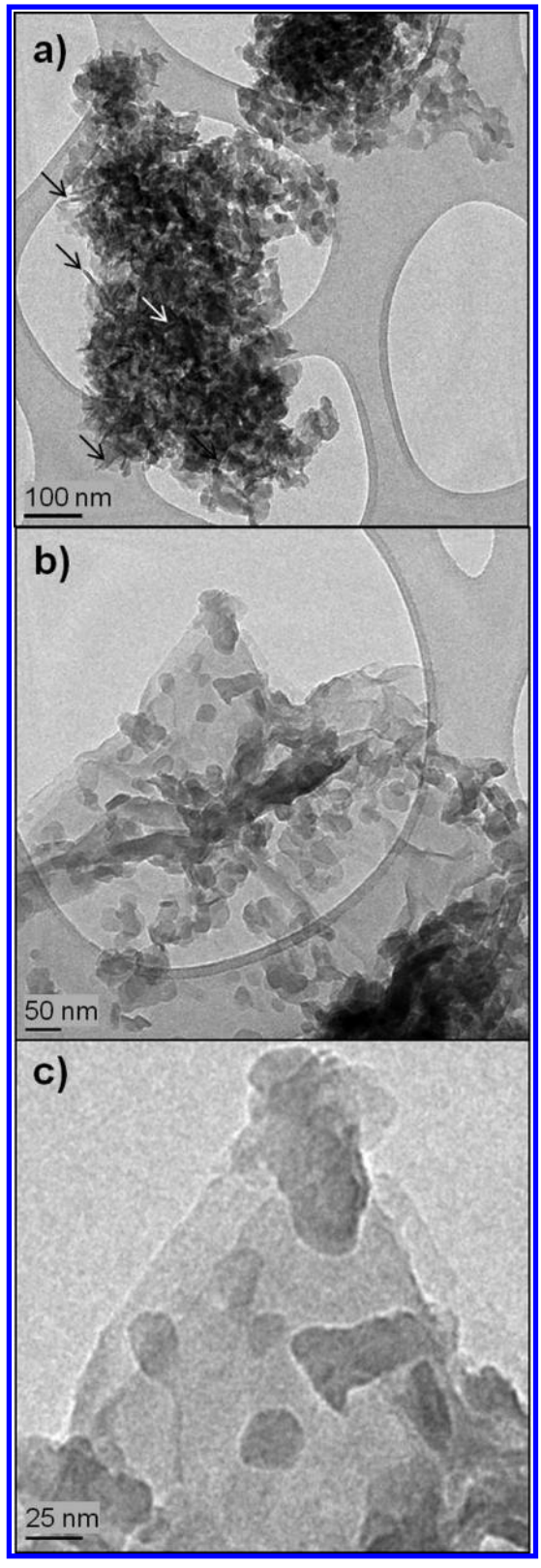

Figure 3. At increasing magnification (a–c) HRTEM images of the [1/1] LDH/GO sample. Examples of edge-on platelets indicated by arrows in (a).

dx.doi.org/10.1021/cm3018264 | *Chem. Mater.* 2012, 24, 4531–4539

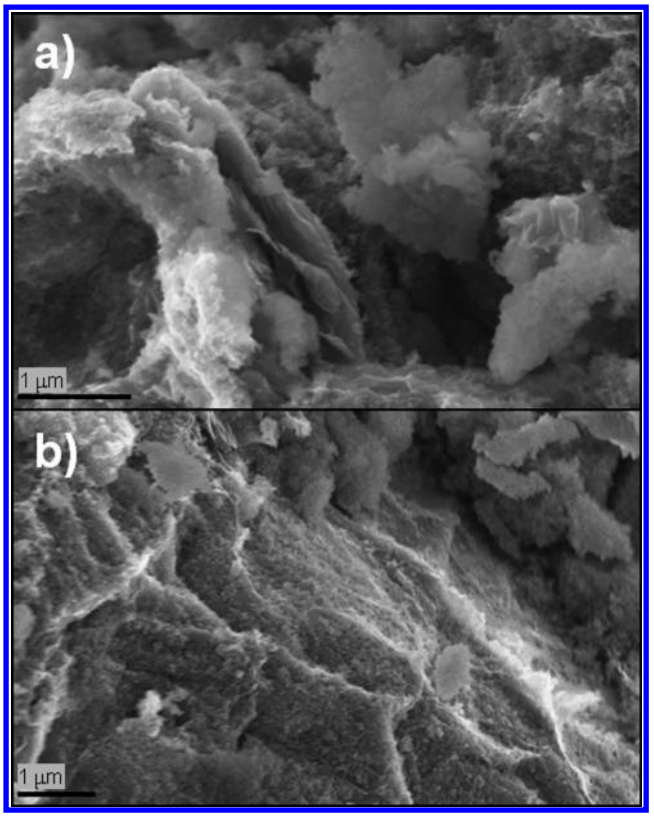

Figure 4. Representative SEM images of (a) as-synthesized and (b) calcined [1/1] LDH/GO sample.

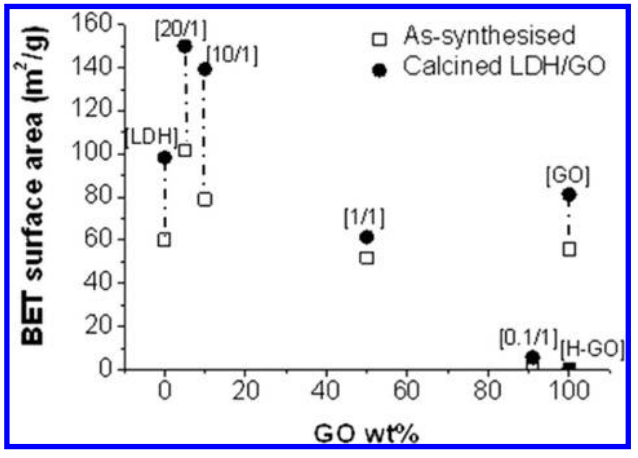

Figure 5. BET surface area as a function of GO weight percentage for the as-synthesized and calcined LDH/GO samples and for the hydrothermally treated GO (H-GO).

The pore-size distribution shows an average of 15 to 19 nm for all samples. The mesopore volume (see Supporting Information) increases with increasing LDH concentration following the same trend as that observed for the BET surface area. Therefore, the increase in the surface area is related to the increasing number of mesopores as small LDH platelets are incorporated with the hybrid.

The calcination of the LDH samples resulted in mixed metal oxides (MMOs) with weak broad peak reflections in the XRD patterns (Figure 6) at 37°, 43°, and 62°, which correspond to diffraction by the (111), (200), and (220) planes related to periclase (MgO, JCPDS No. 45-946). The calcination of the GO led to XRD patterns with graphitic (002) and (100) lattice

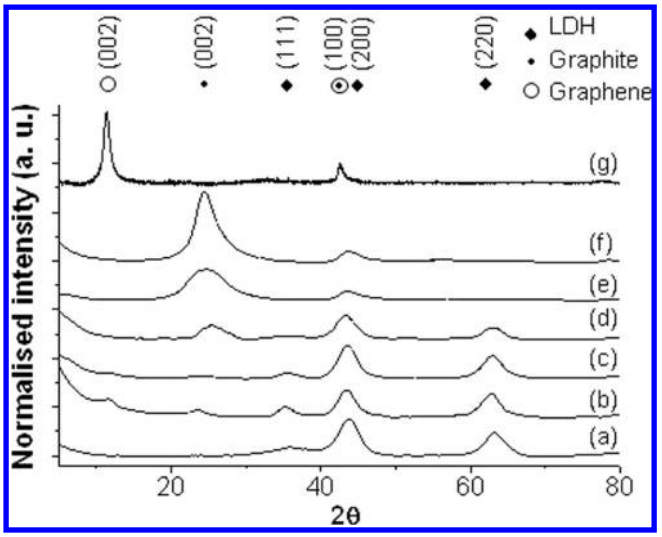

Figure 6. XRD diffraction patterns of (a) unsupported calcined LDH, (b) calcined [20/1] LDH/GO (5 wt % GO), (c) [10/1] LDH/GO (9 wt % GO), (d) [1/1] LDH/GO (50 wt % GO), (e) [0.1/1] LDH/GO (91 wt % GO), (f) calcined GO, and (g) as synthesized GO.

planes in similar positions to H-GO (Figure 1f) but with greater definition. It is likely that the GO sheets were partially, thermally reduced during the calcination process.[35] The presence of the graphite (002) reflections in the calcined [0.1/1] and [1/1] samples indicates that, at these concentrations, the LDH does not prevent all restacking; although again the breadth of the graphitic (002) in the hybrid samples is significantly increased.

The application of the synthesized LDHs to temperature swing processes, such as precombustion carbon capture and storage (CCS) and sorption-enhanced hydrogen production, requires optimization of the adsorption and regeneration temperatures. A low adsorption temperature and high regeneration temperature gives maximum adsorption capacity, but is energy inefficient and leads to large thermal gradients. In general, use of intermediate adsorption temperatures and low regeneration gradients are more favorable for industrial application. Consequently, in the current work, representative adsorption and desorption temperatures of 573 and 673 K respectively were used to assess the performance of the hybrids. The TGA (Figure 2) showed a finite weight loss from the GO above 700 K, suggesting a limit for long-term stability of the system. Temperature programmed desorption of CO_2 (CO_2-TPD) showed that the activated (calcined) LDH has three main types of basic sites that correspond to the formation of bicarbonates, bidentate, and monodentate carbonates, and desorb at temperatures of 423, 543, and 813 K respectively (see Figure 10 in Garcia-Gallastegui et al., 2012).[9] Under the operating regime used here, therefore, it is mainly the desorption state centered at 543 K that is cyclically populated and depopulated.

The CO_2 adsorption curves at 573 K of the unsupported and GO-supported LDHs showed an initial fast increase in adsorption followed by a slower uptake process. For practical purposes, the adsorption capacities reported here correspond to 120 min after CO_2 exposure since the adsorption profile of the materials was essentially steady. At the measurement temperature, the contribution of graphene oxide to the adsorption capacity of the supported materials was found to be negligible.

dx.doi.org/10.1021/cm3018264 | Chem. Mater. 2012, 24, 4531−4539

The adsorption capacities of the materials were determined as the average of at least 3 measurements under the same operating conditions. The adsorption capacity of the pure LDH and the hybrid with the highest LDH/GO ratio [20/1] showed good reproducibility, whereas the other supported LDHs exhibited more variable adsorption capacities (Figure 7). This

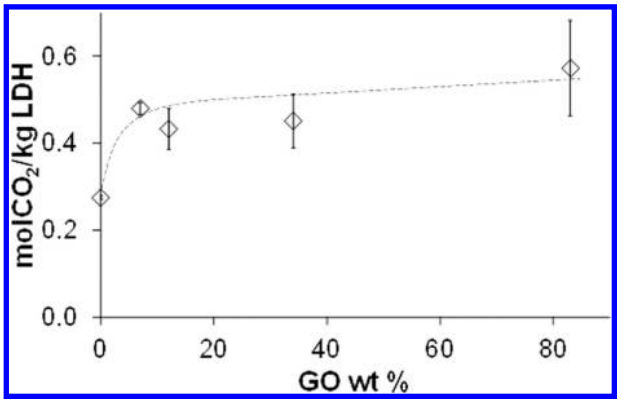

Figure 7. Average CO_2 sorption capacities per mass of LDH at 573 K and $P(CO_2)$ = 0.2 bar, based on measured GO content, shown with standard errors.

variation can be attributed to heterogeneity in the material (particularly in terms of packing) on the scale of mass used for TGA (5 mg), and is greater as the GO content in the sample increases. However, Figure 7 shows clearly that the mean adsorption capacity per mass of LDH is significantly increased (by 74%) on adding a small amount of GO (7 wt %). Any modest further increase, at greater GO content, is less than the error. This trend (Figure 7; Table 1) is associated with a decrease in the apparent size, or coherence length, in the *c*-direction (layer-stacking direction) from 30 nm in the unsupported LDH to 10 nm in the LDH/GO samples (estimated by the Scherrer equation). The enhancement in adsorption capacity in the presence of GO can be attributed to these thinner LDH platelets and their dispersion/stabilization on a compatible support, leading to increases in active/effective LDH surface area. The geometric and electrostatic compatibility between LDH and GO appears to favor heterogeneous nucleation, dispersion, and stabilization; while the XRD broadening might be associated with a greater concentration of defects and hence active sites,[36] the TEM data indicates that physically thinner platelets are the dominant effect. In our previous work based on carbon nanotubes/LDH hybrids,[9] we observed that, in the absence of carboxylic acid groups on the nanotubes, the performance of the CO_2 adsorption of the hybrid was not improved; the equivalent control cannot be performed on "unoxidized GO", as graphite has negligible surface area for LDH deposition; however, the surface chemistry is analogous. Unlike LDHs supported on MWNTs, the sorption enhancement saturates, rather than increasing with increasing dilution onto the GO support; the reason is probably the relatively poor network-forming ability of GO and the tendency to restack, reducing the surface area of the adsorbents. On the other hand, the adsorption capacities per mass of LDH determined in this study are significantly higher than for LDHs supported on MWNTs (0.35−0.4 mol CO_2/kg LDH)[9] at relatively low carbon contents and under the same operating conditions. Meis et al.[36] reported higher CO_2 capacities for very dilute LDHs supported on carbon nanofibers (1.3−2.5 mol CO_2/kg LDH). However, these values are not directly comparable with the GO and MWNTs studies since the CO_2 adsorption was carried out in the presence of water, which is known to increase significantly the adsorption capacity of LDHs,[5,6,37] and at lower adsorption temperature.

In terms of adsorption capacity normalized with respect to the total mass of adsorbent, an optimum loading of LDH can be expected that takes advantage of improved dispersion and gas accessibility without excessively increasing the total volume of adsorbent needed. Figure 8 shows that this optimum loading

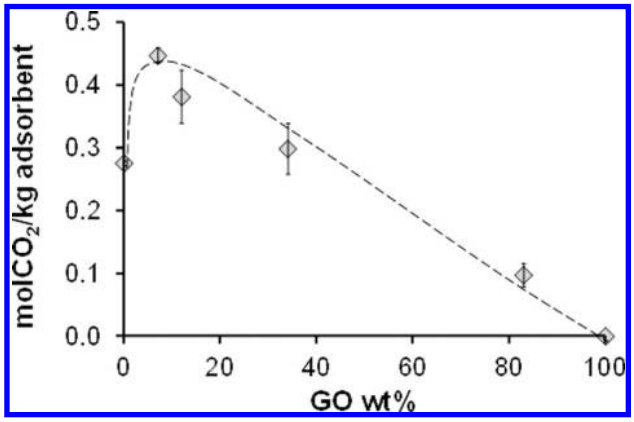

Figure 8. Average CO_2 sorption capacities per mass of total adsorbent of pure LDH and carbon hybrids at 573 K and $P(CO_2)$ = 0.2 bar, based on measured GO content, shown with standard errors.

corresponds to 5−10 wt % GO. The synthesized hybrid containing 7 wt % of GO is within this range and exhibits an absolute capacity 62% higher (based on total mass of adsorbent) than that of the pure LDH (Table 1 and Figure 8). Compared with LDHs supported on MWNTs, much lower amounts of carbon support are needed to achieve a maximum adsorption capacity per mass of total adsorbent (compare 7 wt % GO and 38 wt % MWNTs).[9] In addition, the adsorption capacities (per mass of total adsorbent) of the GO hybrids are considerably higher than the corresponding capacities of the MWNT-supported LDHs.[9]

Continuous adsorption−desorption cycles provide an assessment of the regeneration and stability of the pure LDH and the supported LDH containing 7 wt % of GO (Figure 9). The

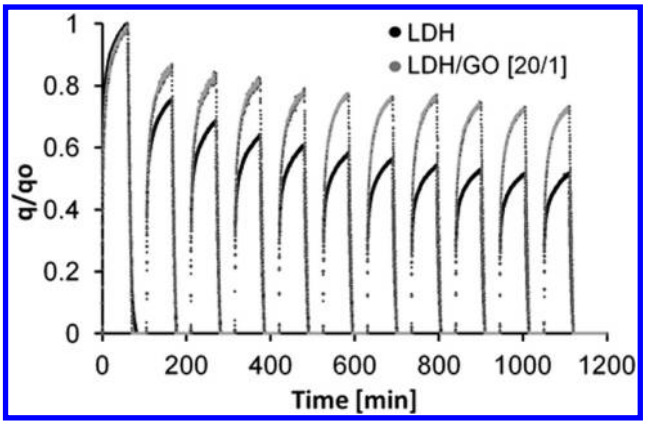

Figure 9. Multicycle profile (adsorption 573 K; desorption 673 K) of the activated LDH (black) and [20/1] LDH/GO (gray) normalized to the first cycle capacity.

dx.doi.org/10.1021/cm3018264 | *Chem. Mater.* 2012, 24, 4531−4539

adsorption capacity of each adsorbent drops markedly during the first cycles and becomes stable gradually. The multicycle profiles observed are consistent with previous research also performed under dry conditions, which have attributed the initial loss of capacity to a small amount of CO_2 irreversibly chemisorbed in the LDH.[5,6,38] The stability of the unsupported LDH is greatly improved by the addition of 7 wt % of GO, Figure 10; after 11 cycles, the adsorption capacity of the carbon

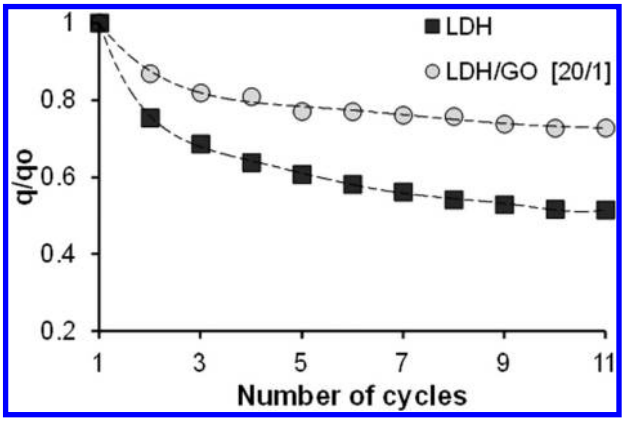

Figure 10. Normalized CO_2 adsorption capacity over 11 adsorption–desorption cycles (adsorption 573 K; desorption 673 K).

hybrid is about 2.5 times higher than that of the pure LDH. This significant result emphasizes the potential of LDH/GO hybrids containing low amounts of GO for CO_2 capture processes. Both capacity and stability are proved to increase, as hypothesized. The changes are linked to dispersion as shown by microscopy (Figures 3 and 4), changes in effective surface area (Figure 5), and LDH thickness (Figure 1). Water has been reported to mitigate the initial loss in CO_2 adsorption capacity observed under dry conditions,[6,36] and future studies of the performance of the LDH/GO hybrids are planned under humidified atmospheres.

4. CONCLUSIONS

During the precipitation of positively charged Mg–Al LDH onto negatively charged GO, the mutual electrostatic interactions drive the self-assembly of heterostructured nanohybrids, in a "layer-by-layer" fashion.[39] The resultant LDH serves as a spacer to prevent aggregation of individual graphene sheets, particularly as highly oxidized debris in the GO sample is washed out by aqueous base; conversely, the GO supports the LDH, improving the dispersion, and nucleating a more active structure; the result is a well-dispersed functional LDH–GO hybrid. Subsequent thermal treatment (at 673 K), transforms the Mg–Al hydroxide nanosheets into a useful mixed oxide for gas sorption and catalytic processes. The CO_2 adsorption capacity and multicycle stability of the LDH were both increased when supported onto GO because of enhanced particle dispersion. In particular, the absolute capacity of the LDH was increased by over 60% using only 7 wt % GO as a support. GO appears to be especially effective at supporting LDH, compared to oxidized MWNTs with similar surface chemistry, an effect that can be attributed to the obvious morphological compatibility. The performance also exceeds that of a commercial alumina support tested under equivalent conditions.[9] However, despite the very high efficiency of GO at low contents, further benefits at higher loadings have not yet been obtained because of its poor network forming ability. In the future, approaches to maintain an open GO structure as a support are likely to be beneficial, for example, by critical drying or cross-linking to form an aerogel. Alternatively, combinations of MWNTs and GO will provide a combination of active surface and network formation, as has proved effective in supercapacitor applications.[40] Finally, LDH/GO hybrid structures are likely to be relevant to a wide variety of applications, including CO_2 sorption and catalysis.[41]

■ ASSOCIATED CONTENT

Supporting Information

Mesopore volume distribution for the as-synthesized and calcined LDH/GO samples; adsorption–desorption nitrogen isotherm of the LDH, GO and as-synthesized LDH/GO samples; EDS results for the LDH and LDH/GO samples. This material is available free of charge via the Internet at http://pubs.acs.org.

■ AUTHOR INFORMATION

Corresponding Author

*E-mail: m.shaffer@imperial.ac.uk (M.S.P.S.), ainara.garcia@bio-nano-consulting.com (A.G.-G.).

Author Contributions

Concepts for the research program were conceived by all authors. Experiments were devised by M.S. and D.C., together with A.G.G., D.I., and V.G. who carried them out and performed data analysis. All authors have given approval to the final version of the manuscript.

Notes

The authors declare no competing financial interest.

■ ACKNOWLEDGMENTS

The authors are grateful to Felicity Sartain, Stephen Hodge, Almudena Celaya-Sanfiz, Maurice C. D. Mourad, and Neal Skipper, for discussions and help during experiments. Financial support for this project was provided by the Deanship of Scientific Research at King Abdulaziz University T/81/429 and scholarships from CONACYT and SEP.

■ ABBREVIATIONS

LDHs, layered double hydroxides; GO, graphene oxide; H-GO, hydrothermally treated GO; MWNTs, multiwalled carbon nanotubes; MMOs, mixed metal oxides; CCS, carbon capture and storage; XRD, X-ray diffraction; TGA, thermogravimetric analysis; SEM, scanning electron microscopy; HRTEM, high resolution transmission electron microscopy; EDS, energy dispersive X-ray spectrometer; ICP-AES, inductively coupled plasma atomic emission spectroscopy; BET, Brunauer, Emmett and Teller

■ REFERENCES

(1) Compton, O. C.; Nguyen, S. T. *Small* **2010**, *6* (6), 711–723.
(2) Allen, M. J.; Tung, V. C.; Kaner, R. B. *Chem. Rev.* **2009**, *110* (1), 132–145.
(3) Dreyer, D. R.; Park, S.; Bielawski, C. W.; Ruoff, R. S. *Chem. Soc. Rev.* **2010**, *39* (1), 228–240.
(4) Choi, S.; Drese, J. H.; Jones, C. W. *ChemSusChem* **2009**, *2* (9), 796–854.
(5) Hufton, J. R.; Mayorga, S.; Sircar, S. *AIChE J.* **1999**, *45* (2), 248–256.
(6) Ding, Y.; Alpay, E. *Chem. Eng. Sci.* **2000**, *55* (17), 3461–3474.
(7) Ding, Y.; Alpay, E. *Chem. Eng. Sci.* **2000**, *55* (18), 3929–3940.

(8) van Selow, E. R.; Cobden, P. D.; Verbraeken, P. A.; Hufton, J. R.; van den Brink, R. W. *Ind. Eng. Chem. Res.* **2009**, *48* (9), 4184−4193.
(9) Garcia-Gallastegui, A.; Iruretagoyena, D.; Mokhtar, M.; Asiri, A. M.; Basahel, S. N.; Al-Thabaiti, S. A.; Alyoubi, A. O.; Chadwick, D.; Shaffer, M. S. P. *J. Mater. Chem.* **2012**, *22* (28), 13932−13940.
(10) Zhao, M.-Q.; Zhang, Q.; Huang, J.-Q.; Wei, F. *Adv. Funct. Mater.* **2012**, *22* (4), 675−694.
(11) Chen, D.; Wang, X.; Liu, T.; Wang, X.; Li, J. *ACS Appl. Mater. Interfaces* **2010**, *2* (7), 2005−2011.
(12) Wu, X.-L.; Wang, L.; Chen, C.-L.; Xu, A.-W.; Wang, X.-K. *J. Mater. Chem.* **2011**, *21* (43), 17353−17359.
(13) Wang, Y. L.; Peng, W.; Liu, L.; Tang, M.; Gao, F.; Li, M. G. *Microchim. Acta* **2011**, *174* (1−2), 41−46.
(14) Li, H.; Zhu, G.; Liu, Z.-H.; Yang, Z.; Wang, Z. *Carbon* **2010**, *48* (15), 4391−4396.
(15) Park, W. I.; Lee, C.-H.; Lee, J. M.; Kim, N.-J.; Yi, G.-C. *Nanoscale* **2011**, *3* (9), 3522−3533.
(16) Latorre-Sanchez, M.; Atienzar, P.; Abellán, G.; Puche, M.; Fornés, V.; Ribera, A.; García, H. *Carbon* **2012**, *50* (2), 518−525.
(17) Dong, X.; Wang, L.; Wang, D.; Li, C.; Jin, J. *Langmuir* **2011**, *28* (1), 293−298.
(18) Nethravathi, C.; Rajamathi, M.; Ravishankar, N.; Basit, L.; Felser, C. *Carbon* **2010**, *48* (15), 4343−4350.
(19) Li, M.; Zhu, J. E.; Zhang, L.; Chen, X.; Zhang, H.; Zhang, F.; Xu, S.; Evans, D. G. *Nanoscale* **2011**, *3* (10), 4240−4246.
(20) Gao, Z.; Wang, J.; Li, Z.; Yang, W.; Wang, B.; Hou, M.; He, Y.; Liu, Q.; Mann, T.; Yang, P.; Zhang, M.; Liu, L. *Chem. Mater.* **2011**, *23* (15), 3509−3516.
(21) Wang, H.-W.; Hu, Z.-A.; Chang, Y.-Q.; Chen, Y.-L.; Wu, H.-Y.; Zhang, Z.-Y.; Yang, Y.-Y. *J. Mater. Chem.* **2011**, *21* (28), 10504−10511.
(22) Wang, L.; Wang, D.; Dong, X. Y.; Zhang, Z. J.; Pei, X. F.; Chen, X. J.; Chen, B.; Jin, J. *Chem. Commun.* **2011**, *47* (12), 3556−3558.
(23) Huang, S.; Zhu, G.-N.; Zhang, C.; Tjiu, W. W.; Xia, Y.-Y.; Liu, T. *ACS Appl. Mater. Interfaces* **2012**, *4* (4), 2242−2249.
(24) Zhang, L.; Zhang, X.; Shen, L.; Gao, B.; Hao, L.; Lu, X.; Zhang, F.; Ding, B.; Yuan, C. *J. Power Sources* **2012**, *199* (0), 395−401.
(25) Yang, J. I.; Kim, J. N. *Korean J. Chem. Eng.* **2006**, *23* (1), 77−80.
(26) Reddy, M. K. R.; Xu, Z. P.; Lu, G. Q.; da Costa, J. C. D. *Ind. Eng. Chem. Res.* **2006**, *45* (22), 7504−7509.
(27) Hu, H.; Bhowmik, P.; Zhao, B.; Hamon, M. A.; Itkis, M. E.; Haddon, R. C. *Chem. Phys. Lett.* **2001**, *345* (1−2), 25−28.
(28) Verdejo, R.; Lamoriniere, S.; Cottam, B.; Bismarck, A.; Shaffer, M. *Chem. Commun.* **2007**, *5*, 513−515.
(29) Park, S.; Lee, K.-S.; Bozoklu, G.; Cai, W.; Nguyen, S. T.; Ruoff, R. S. *ACS Nano* **2008**, *2* (3), 572−578.
(30) Peigney, A.; Laurent, C.; Flahaut, E.; Bacsa, R. R.; Rousset, A. *Carbon* **2001**, *39* (4), 507−514.
(31) Zhao, H. T.; Nagy, K. L. *J. Colloid Interface Sci.* **2004**, *274* (2), 613−624.
(32) Millange, F.; Walton, R. I.; O'Hare, D. *J. Mater. Chem.* **2000**, *10* (7), 1713−1720.
(33) Rourke, J. P.; Pandey, P. A.; Moore, J. J.; Bates, M.; Kinloch, I. A.; Young, R. J.; Wilson, N. R. *Angew. Chem., Int. Ed.* **2011**, *50* (14), 3173−3177.
(34) Zhou, Y.; Bao, Q.; Tang, L. A. L.; Zhong, Y.; Loh, K. P. *Chem. Mater.* **2009**, *21* (13), 2950−2956.
(35) Ding, J. N.; Liu, Y. B.; Yuan, N. Y.; Ding, G. Q.; Fan, Y.; Yu, C. T. *Diamond Relat. Mater.* **2012**, *21* (0), 11−15.
(36) Meis, N.; Bitter, J. H.; de Jong, K. P. *Ind. Eng. Chem. Res.* **2010**, *49* (3), 1229−1235.
(37) Reddy, M. K. R.; Xu, Z. P.; Lu, G. Q.; da Costa, J. C. D. *Ind. Eng. Chem. Res.* **2008**, *47* (8), 2630−2635.
(38) Hutson, N. D.; Attwood, B. C. *Adsorption* **2008**, *14* (6), 781−789.
(39) Ariga, K.; Hill, J. P.; Lee, M. V.; Vinu, A.; Charvet, R.; Acharya, S., . *Sci. Technol. Adv. Mater.* **2008**, *9*, (1).
(40) Mishra, A. K.; Ramaprabhu, S. *AIP Advances* **2012**, *2* (2), 022121.
(41) Xu, Z. P.; Zhang, J.; Adebajo, M. O.; Zhang, H.; Zhou, C. *Appl. Clay Sci.* **2011**, *53* (2), 139−150.